

NUCLEAR SEGMENTATION IN MICROSCOPE CELL IMAGES: A HAND-SEGMENTED DATASET AND COMPARISON OF ALGORITHMS

Luís Pedro Coelho^{1,2,3}, Aabid Shariff^{1,2,3}, Robert F. Murphy^{1,2,3,4,5}

¹Lane Center for Computational Biology, Carnegie Mellon University

²Center for Bioimage Informatics, Carnegie Mellon University

³Joint Carnegie Mellon University–University of Pittsburgh PhD. Program in Computational Biology

⁴Depts. of Biological Sciences, Biomedical Engineering, and Machine Learning, Carnegie Mellon University

⁵External Fellow, Freiburg Institute for Advanced Studies, University of Freiburg, Germany

ABSTRACT

Image segmentation is an essential step in many image analysis pipelines and many algorithms have been proposed to solve this problem. However, they are often evaluated subjectively or based on a small number of examples. To fill this gap, we hand-segmented a set of 97 fluorescence microscopy images (a total of 4009 cells) and objectively evaluated some previously proposed segmentation algorithms.

We focus on algorithms appropriate for high-throughput settings, where only minimal user intervention is feasible.

The hand-labeled dataset (and all software used to compare methods) is publicly available to enable others to use it as a benchmark for newly proposed algorithms.

Index Terms— Biomedical image processing, Image segmentation

1. INTRODUCTION

Nuclear segmentation is an important step in the pipeline of many cytometric analyses. It forms the basis of many simple operations (cell counting, cell-cycle assignment,...) and is often the first step in cell segmentation. However, algorithms are often evaluated subjectively or based on a few examples. In order to objectively evaluate nuclear segmentation algorithms, we built a dataset of hand-segmented fluorescence microscopy images.

We also evaluated some published algorithms for this problem on our hand-labeled dataset. We were interested in algorithms that were applicable to large-scale automated data collection. Therefore, while parameter tuning for the properties of a given image collection was an acceptable burden on the human operator, tuning for single images was not.

Bamford [1] undertook a similar effort in bright-field microscopy images of cell nuclei. Recently, Gelasca et al. [2] made available a series of ground truth assignments for different tasks in bioimage segmentation, but it did not include a dataset of hand-labeled single nuclei. Our dataset is thus a complement to their work.

	U2OS	NIH3T3
Pixel size	1349 × 1030	1344 × 1024
Nr. Cells	1831	2178
Avg. Cover	23%	18%
Min Nr. Cells	24	29
Max Nr. Cells	63	70

Table 1. Main Properties of the Two Collections. Avg. cover denotes the percentage of pixels covered by cells. The minimum and maximum are over all the images in each collection.

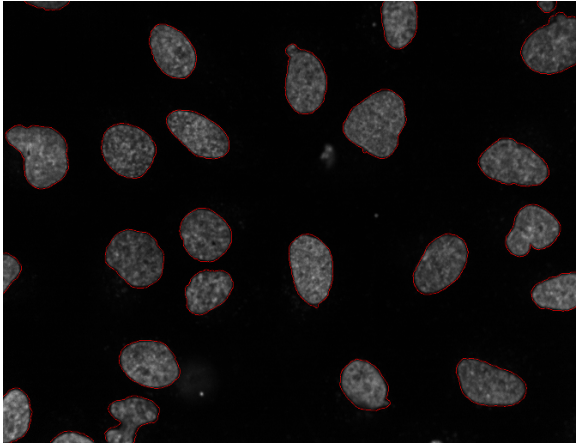
2. DATASET

The dataset is composed of two different collections (Table 1). The first collection is of U2OS cells, originally created for a study of pattern unmixing algorithms [3]. Figure 1 shows two images from this collection. An initial set of 50 images from this collection was chosen, but 2 images were rejected as containing no in-focus cells.

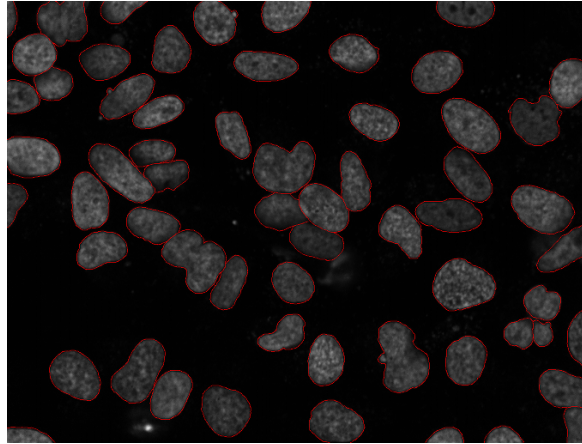
The second collection is of NIH3T3 cells, collected using the methodology reported by Osuna et al. [4]. Nuclei in this group are further apart and there is less clustering. They are also more homogeneous in shape and size (data not shown). On the other hand, nuclei in single images vary greatly in brightness and images often contain visible debris. Therefore, we consider this a more challenging dataset for automated methods. Fifty images were initially chosen, but one was rejected as containing no in-focus cells.

Manual segmentation was performed by outlining nuclei with a computer mouse. Only the nuclear marker image was used for this process. All images were segmented by one of the authors (L.P.C.) and a subset of 10 images (5 from each collection) were independently segmented by another (A.S.).

The hand-labeled dataset and all software necessary to generate the results in this paper are available at <http://murphy-lab.web.cmu.edu/data> and <http://murphy-lab.web.cmu.edu/software>.



(a) “Easy” image



(b) “Difficult” image

Fig. 1. Two example images from the U2OS collection. (a) shows nuclei that are well separated. Automatic segmentation is expected to do well. (b) has many clustered nuclei and is expected to challenge segmentation algorithms. Most images in the collection lie in between these two examples.

3. METHODS

3.1. Segmentation

Due to space limitations, we will only describe the ways in which our implementation was adapted to our images and refer the reader to the original publications for detail.

3.1.1. Thresholding

We considered 3 thresholding methods: Ridler-Calvard [5], Otsu [6], and mean pixel value. All above-threshold contiguous regions are considered objects. To remove some noise, we filter the thresholded image with a median filter (window of size 5).

To remove small non-nuclear objects, we filter out objects smaller than 2500 pixels, circa 64 square microns. This post-filtering was applied to all segmentation results in this paper.

3.1.2. Seeded watershed

We implemented two versions of seeded watershed, both run on a thresholded version of the image (using the mean as threshold, which, as we show below, is the better thresholding method for these images). One operates directly on a blurred version of the image¹, while the second one operates on the gradient of the image. In both cases, seeds are regional maxima of the blurred image.

¹We used a gaussian blur with a width of 12 pixels.

3.1.3. Active masks

Active masks are a recent proposal by Srinivasa et al. [7]. The algorithm assumes that there are two classes of objects, foreground and background. Its only parameters are the mean value and standard deviation of the background region.²

Manual tuning led to the following semi-automatic procedure for parameter setting: the value of the background mean is assumed to be the histogram peak plus 3, while the background standard deviation is set to 0.5.

3.1.4. Merging Algorithm

Lin et al. [8] described an algorithm that is based on merging multiple regions obtained from watershed segmentation, using shape information learned from a labeled dataset. We have implemented a slight variation of their algorithm, but retained the structure. In particular, we use the mean method for segmentation, and as shape features: fraction of area that is contained in the convex hull, roundness, eccentricity, area, perimeter, semi-major, and semi-minor axes (all, except the first, computed on the convex hull). Apart from these minor changes, the algorithm is unchanged.

For the studies below, the set segmented by A.S. was used for training and the set segmented by L.P.C. (except the images that are common to both segmentations) were used for testing.

²The active mask framework is more general than this, but we restrict ourselves to the original proposal.

3.2. Evaluation

Several metrics have been proposed for evaluation of segmentation results against a hand-labeled standard. Some approaches stem from viewing segmentation as a form of clustering of pixels. This allows the use of metrics developed for the evaluation of clustering results. From this family of approaches, we used the Rand and Jaccard indices [9, 10].

The disadvantage of such metrics is that they do not take into account the spatial characteristics of segmentation. In fact, the exact location of the border between foreground and background is often fuzzy. An algorithm that returns a nucleus which almost matches the gold-standard except for a one-pixel-wide sliver around the border should be judged very highly even if that sliver contains a large number of pixels. Previous work on evaluation of bright-field microscopy images by Bamford [1] used the Hausdorff metric.

3.2.1. The Rand and Jaccard Indices

Let S be a (binary) segmented image and R be a (binary) reference image. Let i and j range over all pairs of pixels where $i \neq j$, then each pair falls into one of four categories: (a) $R_i = R_j$ and $S_i = S_j$, (b) $R_i \neq R_j$ and $S_i = S_j$, (c) $R_i = R_j$ and $S_i \neq S_j$, (d) $R_i \neq R_j$ and $S_i \neq S_j$. If we let a, b, c, d refer to the number of pairs in its corresponding category, then the Rand index is defined as:

$$RI(R, S) = \frac{a + d}{a + b + c + d}. \quad (1)$$

That is, the Rand index measures the fraction of the pairs where the two clusterings agree. The Rand index ranges from 0 to 1, with 1 corresponding to perfect agreement.

Based on the same definitions for a, b, c, d , the Jaccard index is defined as:

$$JI(R, S) = \frac{a + d}{b + c + d}. \quad (2)$$

The Jaccard index is not upper-bounded, but higher values correspond to better agreement.

3.2.2. Error Counting

Each object in the segmented image is assigned to the object in the reference image with which it shares the most pixels. Based on these assignments, we can define the following classes of errors: **split**: two segmented nuclei are assigned to a single reference nucleus; **merged**: two reference nuclei are assigned to a single segmented nucleus; **added**: a segmented nucleus is assigned to the reference background; and **missing**: a reference nucleus is assigned to the segmented background.

3.2.3. Spatially-Aware Evaluation Methods

We implemented two spatially-aware evaluation metrics. Both are based on assigning segmented nuclei to reference nu-

clei as above, as they are computed between pairs of matched objects.

For each pixel, we compute its distance to the reference border. The normalised sum of distances is then defined as:

$$NSD(R, S) = \frac{\sum_i \mathbb{I}[R_i \neq S_i] * D(i)}{\sum_i D(i)}, \quad (3)$$

where the sum index i ranges over pixels in the union of both objects and $D(i)$ is the distance of pixel i to the border of the reference object. From the equation, it is obvious that $NSD(R, S) \in [0, 1]$, with 0 corresponding to perfect agreement and 1 to no-overlap. We note that the sum of distances is *not* a metric as it is neither symmetric nor does it satisfy the triangle inequality.

The Hausdorff metric is computed as described by Bamford [1]. In the notation above it can be defined as:

$$H(R, S) = \max \{D(i) : S_i \neq R_i\}. \quad (4)$$

4. RESULTS

Table 2 summarises the results obtained.

Both manual segmentations are in general agreement. Disagreements can be tracked down to an image where the authors differed on whether some small bright objects should be marked as nuclei or debris.

Both Otsu and Ridler-Calvard thresholding score poorly, missing many cells, particularly in the NIH3T3 collection. In this collection, the presence of very bright cells leads the algorithm to set a threshold between the very bright cells and the rest of the cells, instead of setting it between the foreground and background. The mean thresholding is better suited for these images, which consist mainly of background with objects of very different intensities.

Watershed results in less merges than mean-based segmentation, but more split nuclei and spurious objects. Active masks score poorly mainly due to nuclei over-segmentation and missing objects. Lin et al.'s merging algorithm obtains very good results, dominating other algorithms in almost all metrics.

We also notice the Rand and Jaccard indices while distinguishing the alternative manual segmentation from the automatic ones are not good measures for this data as they fail to distinguish between the better and the worse algorithms. Both the Hausdorff and the NSD measures capture the relationships between the algorithms well.

5. DISCUSSION

We presented a dataset that can be used to evaluate nuclear segmentation algorithms. This dataset consists of two collections, from different cell types and different microscopes.

We also implemented several published algorithms for nuclear segmentation and tested them against our standard. The

Algorithm	RI	Jl	Hausdorff	NSD ($\times 10$)	Split	Merged	Spurious	Missing
AS Manual	95%/93%	2.4/3.4	9.7/12.0	0.5/0.7	1.6/1.0	1.0/1.2	0.8/0.0	2.2/3.2
RC Threshold	92%/77%	2.2/2.1	34.8/26.4	1.2/2.6	1.1/1.0	2.4/2.4	0.3/1.9	5.5/22.1
Otsu Threshold	92%/74%	2.2/2.1	34.9/36.7	1.2/3.5	1.1/0.8	2.4/2.1	0.3/1.7	5.6/26.6
Mean Threshold	96%/82%	2.2/1.9	26.5/24.4	1.0/2.3	1.3/1.4	3.4/5.1	0.9/3.1	3.6/4.8
Watershed (direct)	91%/78%	1.9/1.6	34.9/19.3	3.6/3.7	13.8/2.9	1.2/2.4	2.0/11.6	3.0/5.5
Watershed (gradient)	90%/78%	1.8/1.6	34.6/21.7	3.0/3.8	7.7/2.6	2.0/3.0	2.0/11.4	2.9/5.4
Active Masks	87%/72%	2.1/2.0	148.3/98.0	5.5/5.0	10.5/1.9	2.1/1.5	0.4/3.9	10.8/31.1
Merging Algorithm	96%/83%	2.2/1.9	12.9/15.9	0.7/2.5	1.8/1.6	2.1/3.0	1.0/6.8	3.3/5.9

Table 2. Comparison of Segmentation Algorithms. Result of various segmentation approaches are compared against the hand-segmented standard. Each entry contains two values corresponding to the statistic for two datasets used, U2OS and NIH3T3, respectively.

approach of Lin et al. [8] emerged as the best scoring in most tests. We also concluded that the Hausdorff metric and the normalised sum of distances measure we propose captured the quality of the algorithms better than the alternatives under consideration.

5.1. Acknowledgements

This work was supported in part by NIH grants GM75205 and NSF ITR grant EF-0331657 (R.F.M.). L.P.C. was partially funded by the Fundação Para a Ciência e Tecnologia (grant SFRH/BD/37535/2007) as well as a fellowship from the Fulbright Program.

6. REFERENCES

- [1] P. Bamford, "Empirical comparison of cell segmentation algorithms using an annotated dataset," in *Image Processing, 2003. ICIP 2003. Proc. 2003 International Conference on*, 2003, vol. 2, pp. II-1073-6 vol.3.
- [2] E. D. Gelasca, J. Byun, B. Obara, and B.S. Manjunath, "Evaluation and benchmark for biological image segmentation," in *IEEE International Conference on Image Processing*, Oct 2008, pp. 1816-1819.
- [3] T. Peng, G. M.C. Bonamy, E. Glory, S. K. Chanda D. Rines, and R. F. Murphy, "Automated unmixing of subcellular patterns: Determining the distribution of probes between different subcellular locations," (*Submitted*), 2009.
- [4] E. García Osuna, J. Hua, N. Bateman, T. Zhao, P. Berget, and R. Murphy, "Large-scale automated analysis of location patterns in randomly tagged 3t3 cells," *Annals of Biomedical Engineering*, vol. 35, no. 6, pp. 1081-1087, Jun 2007.
- [5] T. Ridler and S. Calvard, "Picture thresholding using an iterative selection method," *IEEE Transactions on Systems, Man and Cybernetics*, vol. 8, no. 8, pp. 630-632, Aug. 1978.
- [6] N. Otsu, "A threshold selection method from gray-level histograms," *IEEE Transactions on Systems, Man and Cybernetics*, vol. 9, no. 1, pp. 62-66, January 1979.
- [7] G. Srinivasa, M. C. Fickus, M. N. Gonzalez-Rivero, S. Y. Hsieh, Y. Guo, A. D. Linstedt, and J. Kovacevic, "Active mask segmentation for the cell-volume computation and golgi-body segmentation of hela cell images," in *International Symposium on Biomedical Imaging*. 2008, pp. 348-351, IEEE.
- [8] G. Lin, U. Adiga, K. Olson, J. F. Guzowski, C. A. Barnes, and B. Roysam, "A hybrid 3d watershed algorithm incorporating gradient cues and object models for automatic segmentation of nuclei in confocal image stacks," *Cytometry Part A*, vol. 56A, no. 1, pp. 23-36, 2003.
- [9] W. M. Rand, "Objective criteria for the evaluation of clustering methods," *Journal of the American Statistical Association*, vol. 66, no. 336, pp. 846-850, Dec., 1971.
- [10] G. Saporta and G. Youness, "Comparing two partitions: Some proposals and experiments," in *Proc. in Computational Statistics*. 2002, pp. 243-248, Physica Verlag.